



## Full paper

# One-structure-based multi-effects coupled nanogenerators for flexible and self-powered multi-functional coupled sensor systems

Kun Zhao<sup>a,d</sup>, Bangsen Ouyang<sup>a,d</sup>, Chris R. Bowen<sup>b</sup>, Zhong Lin Wang<sup>a,c,d,\*\*</sup>, Ya Yang<sup>a,d,e,\*</sup>

<sup>a</sup> CAS Center for Excellence in Nanoscience, Beijing Key Laboratory of Micro-nano Energy and Sensor, Beijing Institute of Nanoenergy and Nanosystems, Chinese Academy of Sciences, Beijing, 100083, PR China

<sup>b</sup> Department of Mechanical Engineering, University of Bath, BA2 7AK, UK

<sup>c</sup> School of Material Science and Engineering, Georgia Institute of Technology, Atlanta, GA, 30332-0245, USA

<sup>d</sup> School of Nanoscience and Technology, University of Chinese Academy of Sciences, Beijing, 100049, PR China

<sup>e</sup> Center on Nanoenergy Research, School of Physical Science and Technology, Guangxi University, Nanning, 530004, PR China



## ARTICLE INFO

## Keywords:

Electronic skin  
Photovoltaic effect  
Piezoelectric effect  
Pyroelectric effect

## ABSTRACT

The simultaneous monitoring of multi-physical signals is essential for future sensor systems, but is currently only realized by integrating a variety of sensor types into a single device. However, the ability to use a single sensor structure that shares common electrodes can provide a route to multi-functional sensing while also decreasing device size and increasing spatial resolution. Here we report a ferroelectric barium titanate film-based multi-effect coupled nanogenerator for scavenging light, mechanical, and thermal energies to realize a self-powered multi-functional coupled sensor system without using any external power source. The coupled nanogenerator exhibits a strong coupling enhancement with detection sensitivities of 0.42 nA/(mW/cm<sup>2</sup>) during illumination by 405 nm light, 1.43 nA/kPa for pressure detection, and -8.85 nA/K for temperature sensing, where both the light and pressure sensing performances have the highest sensitivities during a cooling temperature variation of ~19.5 K and the largest temperature detection sensitivity can be achieved during strong light illumination of 83.2 mW/cm<sup>2</sup>. Moreover, the coupled nanogenerator array can be integrated into flexible forms for tactile pressure, temperature, and light sensors, and enabling coupled sensing for the development of electronic skins.

## 1. Introduction

With the rapid development of self-powered micro/nanosystems, a variety of nanogenerators based on a range of mechanisms have been widely investigated for scavenging waste energy in the environment. Examples include photovoltaic cells for scavenging solar energy [1–5], piezoelectric nanogenerators for scavenging mechanical energy [6–11] and pyroelectric nanogenerators for scavenging thermal energy [12–16]. Such investigations are important for developing new multi-effect coupled energy materials and exploring the possibility for exploiting coupling effects between different physical properties in the same device structure. Barium titanate (BTO) is a lead-free ferroelectric with an intrinsic spontaneous polarization and demonstrates excellent pyroelectric [17,18] and piezoelectric effects [19–21], which leads to

the generation of charge when subjected to temperature variations and pressures, respectively. Its ferroelectric photovoltaic effect has also been utilized to scavenge solar energy [22–24]. However, the majority of investigations are focused on the development of individual energy harvesters and there have been limited reports on a coupled nanogenerator based on a single structure of BTO to simultaneously scavenge the three energy sources of light, mechanical and thermal energies for self-powered coupled sensor systems. It is necessary to understand the coupling relationships between the different energy scavenging mechanisms and also the effect of coupling on the overall performance of self-powered sensors. Moreover, most of the multi-functional sensor systems are based on the simple integration of individual sensors with different functions due to the possible interactions of the devices. However, the increased cost and increased volume of such multi-device

\* Corresponding author. CAS Center for Excellence in Nanoscience, Beijing Key Laboratory of Micro-nano Energy and Sensor, Beijing Institute of Nanoenergy and Nanosystems, Chinese Academy of Sciences, Beijing, 100083, PR China.

\*\* Corresponding author. CAS Center for Excellence in Nanoscience, Beijing Key Laboratory of Micro-nano Energy and Sensor, Beijing Institute of Nanoenergy and Nanosystems, Chinese Academy of Sciences, Beijing, 100083, PR China.

E-mail addresses: [zhong.wang@mse.gatech.edu](mailto:zhong.wang@mse.gatech.edu) (Z.L. Wang), [yayang@binn.cas.cn](mailto:yayang@binn.cas.cn) (Y. Yang).

<https://doi.org/10.1016/j.nanoen.2020.104632>

Received 21 January 2020; Received in revised form 11 February 2020; Accepted 17 February 2020

Available online 20 February 2020

2211-2855/© 2020 Elsevier Ltd. All rights reserved.

sensor systems limits their application. As a result, the development of a one-structure-based multi-functional coupled sensor system can effectively solve this issue by identifying the detailed coupled relationships between the different sensors.

Here, we report on a one-structure-based nanogenerator that couples photovoltaic, piezoelectric and pyroelectric effects for scavenging 405 nm light, mechanical and thermal energies simultaneously. When subjected to light with an intensity of  $83.2 \text{ mW/cm}^2$ , the coupled current of the nanogenerator under the application of simultaneous illumination and pressure (7.6 kPa) can be enhanced by approximately 387.3% when compared with the output current of the device under light illumination only. When subjected to a temperature decrease of  $\Delta T = -19.5 \text{ K}$ , the output current signal can be enhanced by more than 375.0% when illuminated at an intensity of  $83.2 \text{ mW/cm}^2$ . In addition, the coupled nanogenerator demonstrates excellent stability in terms of output current and exhibits no observable deviation over 100 cycles. Finally, the coupled nanogenerator was deployed in a self-powered multi-functional coupled sensor systems for monitoring light, pressure and temperature variations. Our sensor system stands out among present multi-functional sensor systems [25,26], since a single pixel of our sensor system can simultaneously detect light, pressure and temperature variations which can significantly improve the integration level and reduce cost. When the sensor system is deployed as a  $3 \times 3$  sensor array, it can successfully detect the distribution of light, pressure and temperature. Moreover, its potential application of the system as a sensor skin was demonstrated by mounting the flexible sensor system on a prosthetic hand. Our study exhibits a prospective application of using BTO ceramic for flexible self-powered multi-functional coupled sensor systems.

## 2. Experimental section

### 2.1. Preparation of BTO ceramic wafers

A mass of 0.3 g of BTO nanoparticles was thoroughly mixed with several drops of 2 wt% polyvinyl alcohol (PVA) binder. The obtained fine powders were then transferred to stainless steel mold and compacted into wafers with a diameter of 10 mm under 2.5 MPa. Subsequently, the BTO wafers were sintered at  $650 \text{ }^\circ\text{C}$  for 1 h to eliminate the PVA binder, and then sintered at  $1200 \text{ }^\circ\text{C}$  for 2 h to obtain BTO ceramic wafers.

### 2.2. Fabrications of nanogenerators and sensor systems

A thin layer of Ag was sputtered on the two surfaces of the obtained BTO ceramic wafers using a DC magnetron sputtering system (100 W, 30 min) to act as an electrode. The Ag/BTO/Ag devices were then poled for 30 min under an applied electric field of 2.3 kV/mm in a silicone oil bath at room temperature. Finally, by removing one Ag electrode and polishing the BTO ceramic wafer to approximately  $280 \text{ }\mu\text{m}$ , an ITO electrode was deposited on the polished side of BTO wafer by RF magnetron sputtering for 15 min using a power of 150 W. For the structural layers, the molds (sizes:  $50 \text{ mm} \times 15 \text{ mm} \times 1 \text{ mm}$  and  $50 \text{ mm} \times 50 \text{ mm} \times 1 \text{ mm}$ ) with acrylic sheets were manufactured by processing them as different parts using a laser cutter and bonding the parts together with epoxy. The liquid silicone rubber was obtained by mixing a Sylgard 184 base with curing agents at a mass ratio of 10:1 in a beaker. The liquid silicone was then poured inside the molds with BTO ceramic wafers installed in the center and cured at  $90 \text{ }^\circ\text{C}$  for 1 h. The nanogenerator (NG) was obtained by encapsulating a BTO ceramic wafer in polydimethylsiloxane (PDMS) (mold size:  $50 \text{ mm} \times 15 \text{ mm} \times 1 \text{ mm}$ ). The  $3 \times 3$  matrix flexible sensor systems were assembled by encapsulating nine BTO ceramic wafers in PDMS (mold size:  $50 \text{ mm} \times 50 \text{ mm} \times 1 \text{ mm}$ ).

### 2.3. Characterization and measurements

SEM images were determined using field emission scanning electron microscopy (Hitachi SU8020). The crystal structure of BTO nanoparticles was identified by an X-ray diffractometer (Panalytical X'pert3 powder), using Cu K $\alpha$  radiation. The heating and cooling temperature variations for BTO-PDMS NG and sensor system were achieved by a thermoelectric module positioned below the device, and temperature was monitored using an infrared thermometer (Optris PI400). The illumination intensity was measured by power meter (Nova II Display ROHS) and the applied pressure was determined using a digital dynamometer (ZTA-DPU-50 N). The output current and voltage signals of the nanogenerator and sensor system were measured by a 2611B system source meter. The output voltages of the device were measured under a load resistance of approximately  $100 \text{ }\Omega$ .

## 3. Results and discussion

Fig. 1a is a schematic of the sensor system that acts as a wearable electronic device which can sense light, temperature and pressure signals from the external environment. The multilayered design layout and the corresponding fabrication process of the sensor system is presented in Fig. 1b. Transparent ITO and Ag electrodes were deposited on the upper and bottom surfaces of the BTO ceramic wafers, respectively. Subsequently, the BTO ceramic wafer array was encapsulated in PDMS. Schematics of the final fabricated BTO-PDMS device and sensor system under light illumination are shown in Figs. S1a and S1b (Supporting Information), respectively. Fig. 1c and Fig. S1c (Supporting Information) display the morphology of the BTO nanoparticles with a diameter of approximately 50–100 nm, which were used to fabricate BTO ceramic wafers. As demonstrated in Fig. S1d (Supporting Information), the thickness of the manufactured BTO ceramic wafer after undertaking the processing technologies of dry pressure sintering, polarization and sanding is approximately  $280 \text{ }\mu\text{m}$ . The surface, as seen in Figs. S1e and S1f (Supporting Information), and cross-sectional morphology, Fig. 1d and Fig. S1g (Supporting Information), of the BTO ceramic wafer indicate that the prepared ceramics possess a highly dense microstructure, and the grain size is less than  $5 \text{ }\mu\text{m}$ . X-ray diffraction (XRD) patterns in Fig. S1h (Supporting Information) indicate that the BTO nanoparticles after being calcined at  $1200 \text{ }^\circ\text{C}$  have an orthorhombic phase. Fig. 1e and g presents images of the fabricated BTO-PDMS nanogenerator and sensor system with dimensions of  $50 \text{ mm} \times 15 \text{ mm} \times 1 \text{ mm}$  and  $50 \text{ mm} \times 50 \text{ mm} \times 1 \text{ mm}$ , respectively. As demonstrated in Fig. 1f and h, they exhibit good flexibility when subjected to mechanical deformation.

The output performance of the fabricated device when stimulated independently by light, pressure and temperature were systematically investigated and the data is summarized in Fig. 2. Fig. 2a illustrates the output current signals of the device under periodic illumination by light of a 405 nm wavelength, where the output current increases with an increase in light intensity. The short-circuit current exhibits a large increase from 3.7 nA to 21.6 nA on increasing the light intensity from  $8.39 \text{ mW/cm}^2$  to  $83.2 \text{ mW/cm}^2$ . Since heat is generated during illumination, the output current signals also exhibits a pyroelectric peak, which also increases with an increase in light intensity. The stable curve represents the photovoltaic signal after equilibrium due to the depolarization electric field. In addition, under light illumination, the photo-generated holes flow into the Ag electrode, and the photo-generated electrons diffuse toward the ITO electrode, owing to the influence of internal depolarization field and the Schottky barriers. When light intensity increases, the photo-excited electron-hole pairs are increased so that more holes and free electrons can be collected by the top and bottom electrodes. The output voltage signals of the device under the light illumination can also be observed in Fig. S2a (Supporting Information), which exhibit the same trends as the output current. To confirm that the signals in Fig. 2a and Fig. S2a (Supporting Information) are generated by the BTO-PDMS nanogenerator, the fabricated device was forwardly and

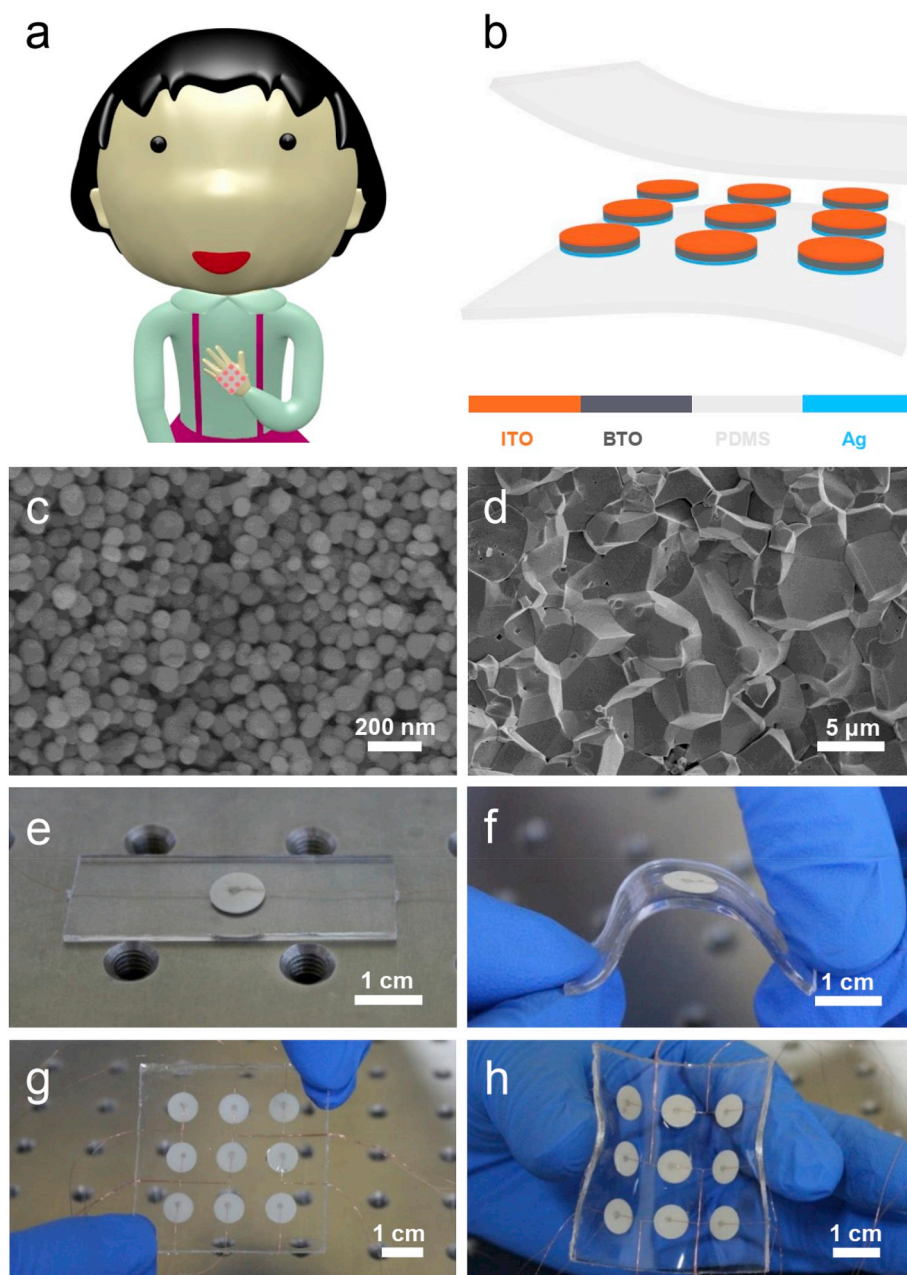


**Fig. 1.** Characterization of the fabricated device. (a) Schematic of the fabricated sensor system for the human body. (b) Schematic of the structure of the fabricated sensor system. (c) SEM image of BTO nanoparticles. (d) Cross-sectional SEM image of BTO ceramic wafer. (e,f) Images of flat (e) and flexed (f) BTO-PDMS device. (g, h) Images of the flat (g) and flexed (h) sensor system.

reversely connected to the measurement system, with positive and negative signals observed when turning on the light see Figs. S2c and S2d (Supporting Information). The corresponding negative signals at reversed connection indicate that the measured signals were generated by the polarized BTO-PDMS nanogenerator.

The output piezoelectric current signals of the BTO-PDMS nanogenerator exhibits a clear increase from 6.5 nA to 21.2 nA as the magnitude of the alternating pressure increases from 7.6 kPa to 33.7 kPa, as demonstrated in Fig. 2b. The mechanism can be interpreted as follows. Due to polarization positive and negative dipole charges in the BTO distribute near the ITO and Ag electrodes, respectively. Under pressure, the device was compressed and a piezoelectric potential pointing from the ITO to the Ag electrode, positive and negative screen charges move to and amass at the two interfaces. Therefore, a negative electric signal is generated in the external circuit. When the applied

pressure is removed, the device is released and the piezoelectric potential disappears. To further confirm that the output signals originate from the direct piezoelectric effect, the output voltage signals of the BTO-PDMS device at forward connection and reversed connection to the measurement system under repeated pressure cycling were measured, see Fig. S2d (Supporting Information). Linear fitting results of the output current of the device under different pressures show that the trend of an increase in current with pressure can be divided into two segments, whose slopes  $k_1$  and  $k_2$  are 0.91 and 0.29, respectively; see Fig. S2e (Supporting Information).

Fig. 2c and Fig. S2f (Supporting Information) display the output current signals for BTO-PDMS nanogenerator when subjected to a range of temperature variations only. The results show that the Ag/BTO/ITO is in the heating state, the electric dipoles in BTO oscillate within a larger angle with their alignment axes, leading to a lower level of effective

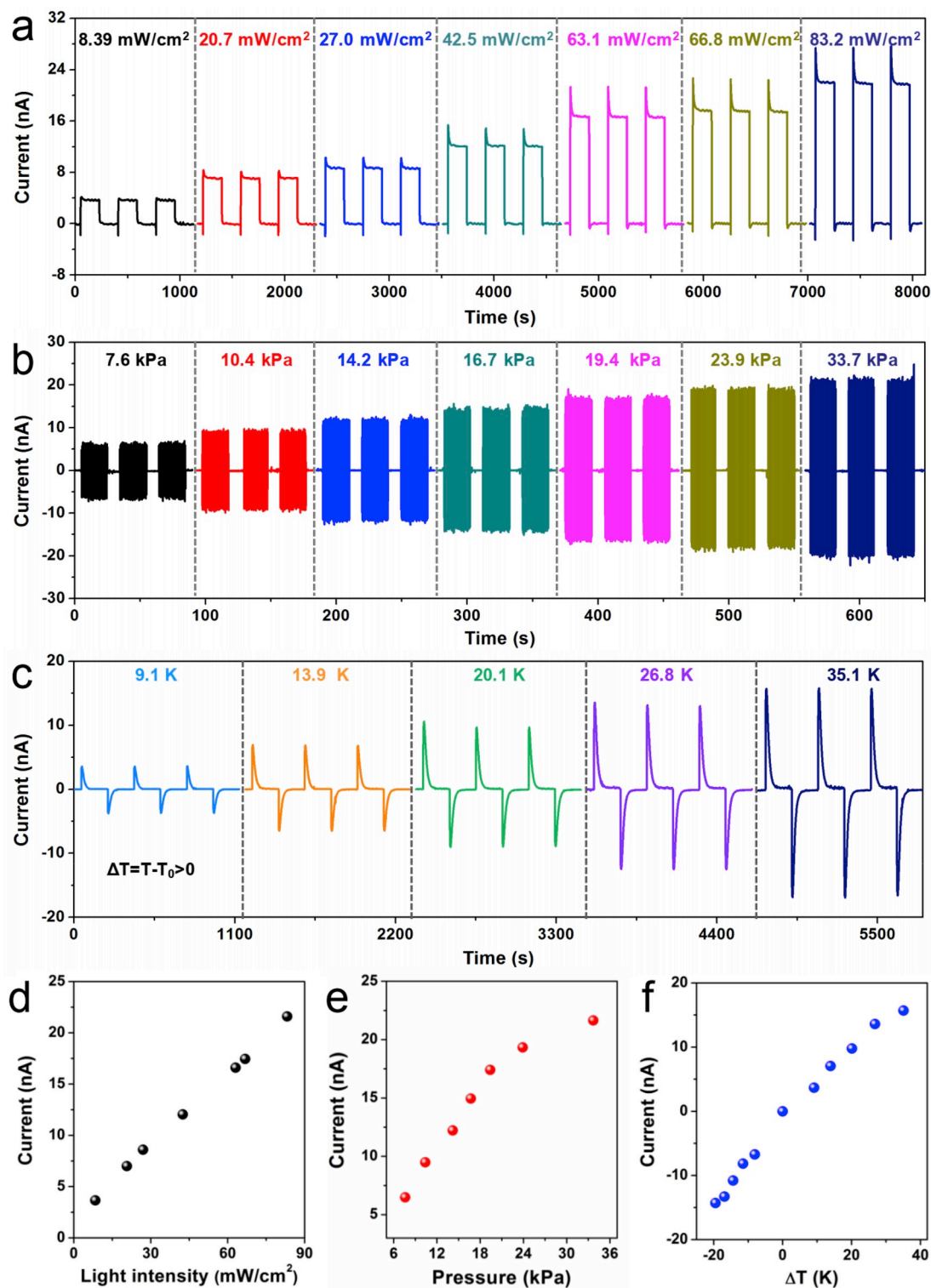


**Fig. 2.** Output performance of the NGs. (a) Measured output current signals for BTO-PDMS device under 405 nm illumination with different intensities from 8.39 mW/cm<sup>2</sup> to 83.2 mW/cm<sup>2</sup>. (b) Measured output current signals for BTO-PDMS device under different pressures from 7.6 kPa to 33.7 kPa. (c) Measured output current signals for BTO-PDMS device under different heating temperature variations from 9.1 K to 35.1 K. (d-f) Comparison charts of the measured output current signals of the device under the different illumination intensities (d), pressures (e) and temperature variations (f).

polarization. Therefore, the quantity of induced charges in the electrodes is reduced, resulting in that electrons can flow from the Ag electrode to the ITO electrode. While the Ag/BTO/ITO is in the cooling state, the electric dipoles in BTO will oscillate within a smaller angle with their alignment axes, leading to a higher level of effective polarization. So, the quantity of induced charges in the electrodes is increased,

resulting in an opposite movement of the electrons in the circuit. Thus, the current directions of pyroelectric signals in heating and cooling states are opposite. When heated with a temperature variation of  $\Delta T = 35.1$  K, the output current is approximately 15.7 nA (Fig. 2c), whereas the output current was approximately -14.3 nA when cooled with a temperature variation of  $\Delta T = -19.5$  K (Fig. S2f, Supporting

Information). The temperature-time curves and the corresponding output voltage signals of the nanogenerator under different temperature variation are presented Figs. S3a, S3b, S3d and S3e (Supporting Information), which show that the output voltage signals of the device increase with an increase of heating or cooling temperature variations. The corresponding infrared images of the device at the different temperature variations can be observed by an infrared thermometer, as shown in Fig. S3c (Supporting Information).

To clearly demonstrate the output performance of the fabricated device, the output current under a range light intensities, pressures and temperature variations are summarized in Fig. 2d–f. The result shows that the output current signals of the device increase monotonically with light intensity, pressure and temperature. The output power of the nanogenerator was systematically investigated by connecting the sensor in series with different resistances, as depicted in Fig. S4 (Supporting Information). The maximum output power was obtained at a matched loading resistance with respect to the photovoltaic effect, piezoelectric effect and pyroelectric effect. The maximum output power for the photovoltaic mode of operation is  $\sim 0.81$  nW (33.7 kPa) located at a loading resistance of 4.0 M $\Omega$  (83.2 mW/cm<sup>2</sup>); for the piezoelectric mode the maximum output power is  $\sim 0.19$  nW at a loading resistance of 0.9 M $\Omega$ ; and for the pyroelectric mode the maximum output power is  $\sim 22.4$  nW ( $\Delta T = 39.1$  K) and 25.5 nW ( $\Delta T = -19.5$  K) at loading resistances of 200 M $\Omega$  and 260 M $\Omega$ , respectively. All output current signals decrease with an increase in load resistance since the system is approaching open circuit conditions.

As a key parameter of a sensor, the response speed of the fabricated device was investigated in detail and shown in Figs. S5a–S5c (Supporting Information). The response time and recovery time of the ITO/BTO/Ag structure to illumination by light, pressure and heating was calculated between 10% and 90% of the maximum current signal, respectively. When illuminated by light with a 405 nm wavelength, Fig. S5a (Supporting Information), the response time and the recovery time are approximately 0.68 s and 0.56 s. For the piezoelectric effect, Fig. S5b (Supporting Information), the device exhibits a fast pressure response time and recovery time of 0.03 s and 0.02 s respectively. As shown in Fig. S5c (Supporting Information), the device exhibits a more moderate temperature response time of 2.06 s and recovery time of 32.63 s, respectively due to the slower speed associated with heat transfer. In addition, the stabilities of the fabricated BTO-PDMS nanogenerator under the application of cyclic heating and cyclic pressures were tested, respectively. As demonstrated in Fig. S6 (Supporting Information), the consistent output current signals indicate the excellent stability of the fabricated device to operating conditions.

Due to the multi-functional properties of the BTO-PDMS nanogenerator, it is of interest to investigate the mutual influence between the photovoltaic effect, piezoelectric effect and pyroelectric effect. Fig. 3a and b presents the output current signals of the device under the application of independent heating ( $\Delta T = 35.1$  K) or cooling ( $\Delta T = -19.5$  K) temperature variations, and the application of combined temperature variations and light illumination of different intensities (8.39 mW/cm<sup>2</sup> to 83.2 mW/cm<sup>2</sup>). The result shows that the coupled current of the device under the action of a combined cooling temperature variation ( $\Delta T = -19.5$  K) and illumination (83.2 mW/cm<sup>2</sup>) is 36.1 nA. As a result of the coupling between the ferroelectric effect and photovoltaic effect, when the temperature variation is  $\Delta T = 35.1$  K, the coupled current is reduced to 15.1 nA. The output current signals of the device under the combined application of a range of heating/cooling temperature variations and illuminated with light of different intensities is shown in Figs. S7 and S8 (Supporting Information), respectively. To compare the change of current ( $I_c$ ) under different conditions, the output current signals of the device in Fig. 3a and b, Figs. S7 and S8 (Supporting Information) are summarized in Fig. 3c. The current signal increases monotonically with light intensity for a specific temperature variation ( $\Delta T$ ). It is worth highlighting that the slopes of the fitted current-light intensity lines (detection sensitivity) decrease with an increase of  $\Delta T$

and detailed information can be found in Table S1 (Supporting Information). The detection sensitivity of light of the device can be defined as the change of current value at different light intensity changes. The result shows that the sensitive of the device are 0.42 nA/(mW/cm<sup>2</sup>) and 0.16 nA/(mW/cm<sup>2</sup>) under the light intensities from 8.39 mW/cm<sup>2</sup> to 83.2 mW/cm<sup>2</sup>, respectively.

A heating temperature variation results in the weakening of the output current signals and cooling temperature variation can be utilized to enhance the output current signals of the device, which can be explained by the pyro-phototronic effect [27]. For ferroelectric BTO materials, the spontaneous polarization can be enhanced when it is cooled, resulting in the increase of the internal electric field. As a result, the light-induced electrons and holes can be separated more effectively as compared with that of a higher temperature condition. Figs. S9 and S10 (Supporting Information) display the output voltage signals of the device under the simultaneous application of a temperature change ( $\Delta T$ ) and illumination with light of different intensities. To compare voltage signals of the device under the different condition, the output voltage is further summarized in Fig. S17a (Supporting Information) and shows a clear increase with increasing cooling temperature and decrease with increasing heating temperature variations under a certain light intensity.

Fig. 3d and e, S11 and S12 (Supporting Information) illustrate the output current signals of the device under the application of individual heating and cooling temperature variations, simultaneous application of temperature variations and different alternating pressures from 7.6 kPa to 33.7 kPa. When the heating temperature variation is  $\Delta T = 35.1$  K, the coupled currents of the device under 7.6 kPa and 33.7 kPa are 4.1 nA and 10.0 nA, respectively. When the cooling temperature variation is  $\Delta T = -19.5$  K, the coupled currents of the device under 7.6 kPa and 33.7 kPa are 11.1 nA and 34.8 nA, respectively. By comparison, a heating temperature variation can be utilized to weaken the output current signals and cooling temperature variation can be utilized to enhance the output current signals ( $I_p$ ) of the device, as presented in Fig. 3f. Moreover, the slopes of the currents linear fitting equations (detection sensitivity) increase with an increase of cooling temperature and decreases with the increase of heating temperature variations, respectively, as displayed in Table S2 (Supporting Information). The detection sensitivity of pressure of the device can be regarded as the change of current value at different pressure changes. It is found that the sensitive of the device are 1.43 nA/kPa and 0.38 nA/kPa under the pressures from 7.6 kPa to 33.7 kPa, respectively. Fig. 3g and h, Figs. S13 and S14 (Supporting Information) display the output current signals of the device under the different illumination intensities, simultaneous light illumination and heating/cooling with different temperature variations from 35.1 K to  $-19.5$  K. The coupled currents of the device under the simultaneous light illumination (8.39 mW/cm<sup>2</sup>) and temperature variations (35.1 K or  $-19.5$  K) are 2.2 nA and 7.8 nA. The corresponding coupled currents under the light intensity of 83.2 mW/cm<sup>2</sup> are 14.2 nA and 102.6 nA, respectively. The results indicate that a cooling temperature variation can be utilized to enhance the output current signals of the device under the same light intensity which can be attributed to the pyro-phototronic effect. Moreover, the spontaneous polarization in BTO can be decreased when it was heated, resulting in the decrease of the internal electric field. As a result, it is more difficult for effective separation of electrons and holes as compared to the no heating condition.

The absolute values of the output currents and linear fitting gradient (detection sensitivity) increases with an increase of light intensity, see Fig. 3i and Table S3 (Supporting Information). The detection sensitivities of the device can be considered as the change of current values at the different temperature variation changes. It is obviously that the sensitive of the device are  $-8.85$  nA/K and  $-0.41$  nA/K under the temperature variation from  $-19.5$  to 35.1 K, respectively. The changes of the corresponding voltage signals of the device were consistent with the current, as demonstrated in Figures S15, S16 and S17b (Supporting Information). Moreover, we measured the coupled current of the device

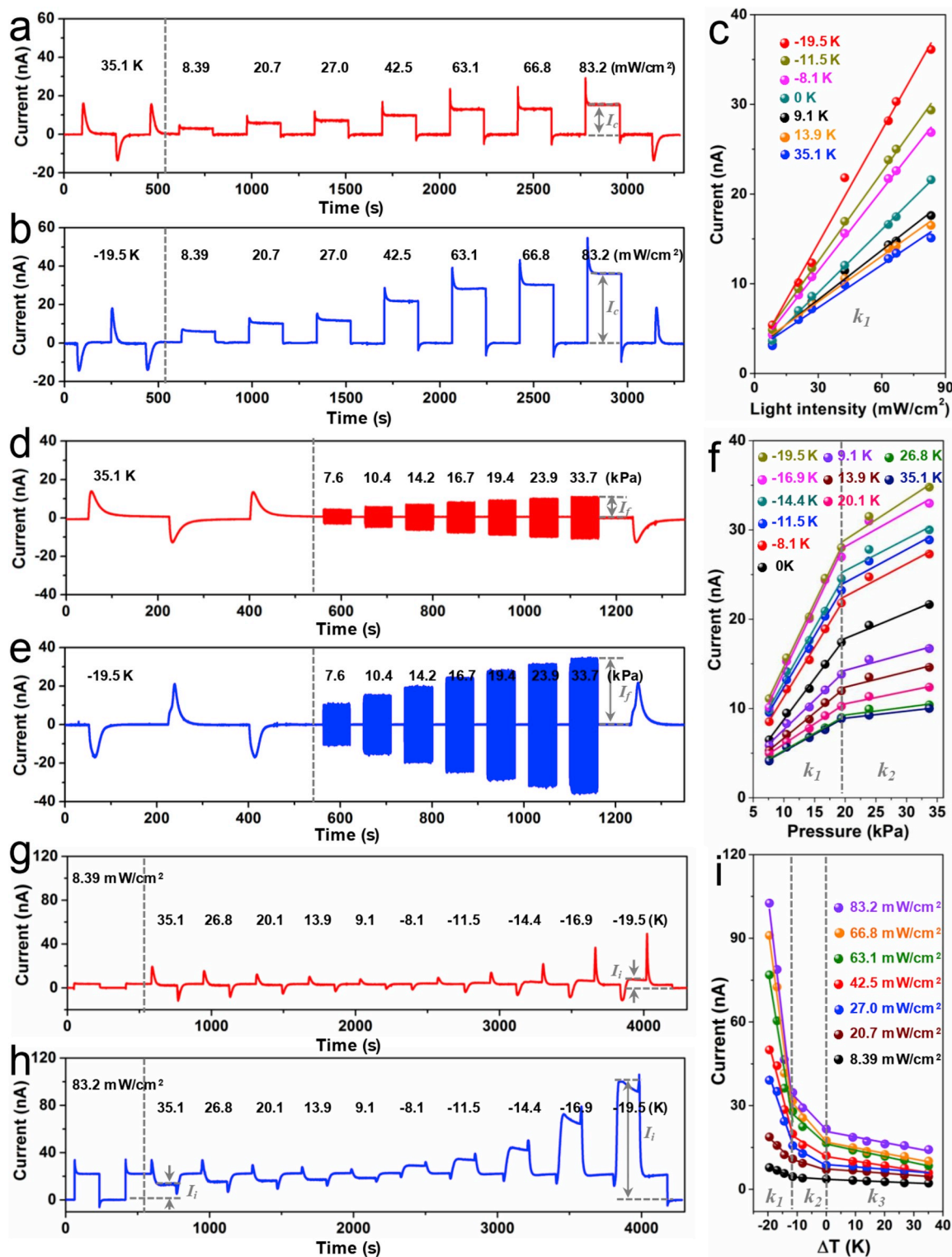
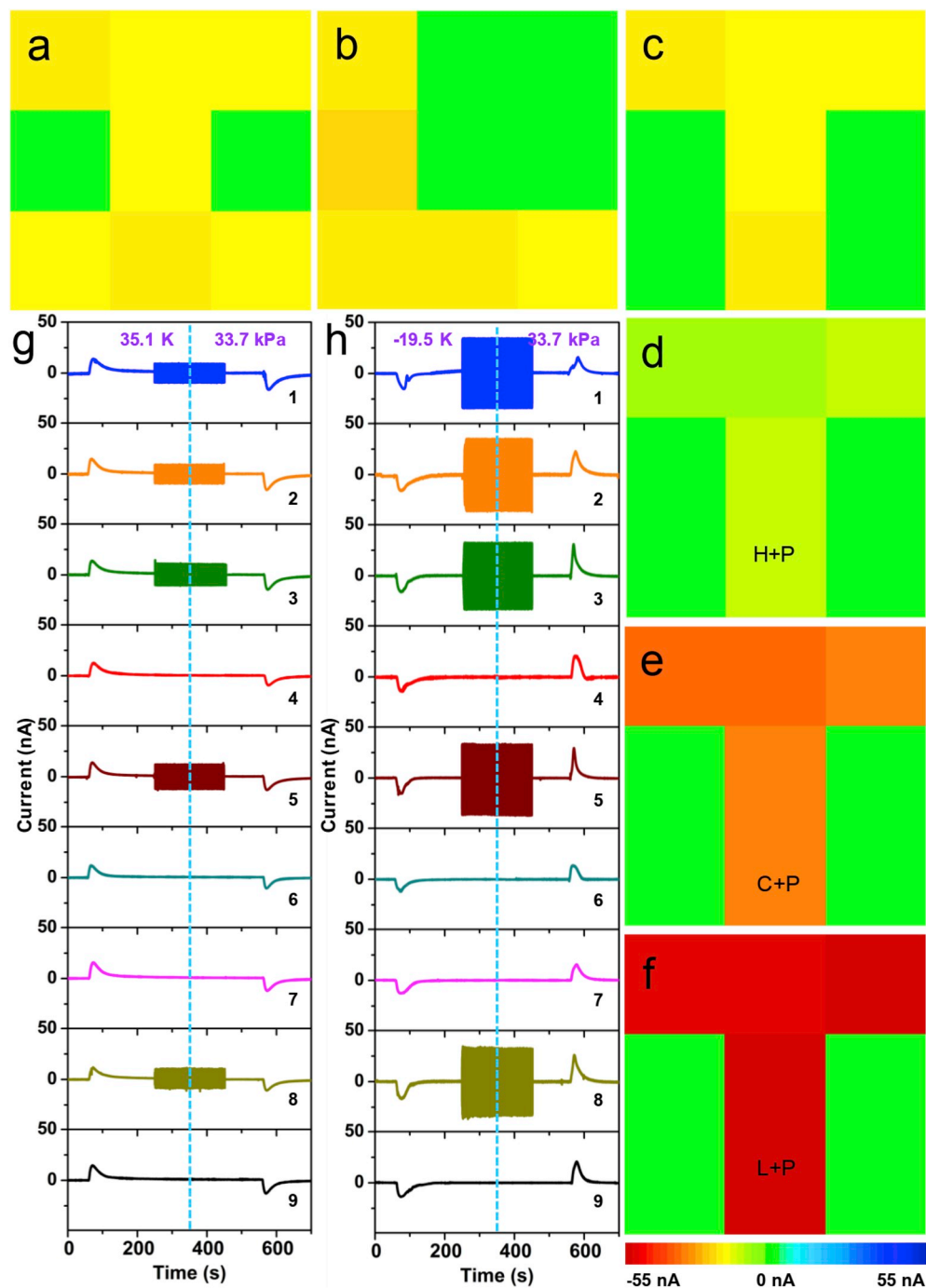


Fig. 3. Multi-effects coupled performance of the NGs. (a,b) Measured output current signals of the device during conditions of heating ( $\Delta T = 35.1$  K) (a) or cooling ( $\Delta T = -19.5$  K) (b) temperature variation and the simultaneous application of a temperature variation and light illumination with different intensities from 8.39 mW/cm<sup>2</sup> to 83.2 mW/cm<sup>2</sup>. (c) Comparison of the measured output current signals of the device under simultaneous heating/cooling at different temperature variations and light illumination with different intensities from 8.39 mW/cm<sup>2</sup> to 83.2 mW/cm<sup>2</sup> (d,e) Measured output current signals of the device under the individual heating ( $\Delta T = 35.1$  K) (d) cooling ( $\Delta T = -19.5$  K) (e) temperature variations and application of simultaneous temperature variations with different pressures from 7.6 kPa to 33.7 kPa. (f) Comparison of the measured output current signals of the device under the simultaneous heating/cooling with different temperature variations and different pressures from 7.6 kPa to 33.7 kPa. (g,h) Measured output current signals of the device under the illumination intensities of 8.39 mW/cm<sup>2</sup> (g) or 83.2 mW/cm<sup>2</sup> (h) and the simultaneous illumination and heating/cooling with different temperature variations from 35.1 K to  $-19.5$  K. (i) Comparison of the measured output current signals of the device under the simultaneous light illumination and heating/cooling with different temperature variations from 35.1 K to  $-19.5$  K.

under the application of simultaneous illumination by light and alternating pressure, as displayed in Figs. S18 and S19 (Supporting Information). The results show that the coupled current is larger than the individual photocurrent. Moreover, the coupling current increases with an increase of light intensity. Under a cooling temperature variation of  $\Delta T = -19.5$  K, the coupled current and voltage of the device under simultaneous cooling temperature variation and light illumination ( $8.39 \text{ mW/cm}^2$ ) was enhanced by  $\sim 47.5\%$  and  $\sim 155\%$  when compared with the current and voltage of the device under individual light illumination, see Figs. S20a and S20b (Supporting Information). Under a light intensity of  $83.2 \text{ mW/cm}^2$ , the coupled current of the device under simultaneous light illumination and pressure ( $7.6 \text{ kPa}$ ) was enhanced by  $\sim 387.3\%$  when compared with the current of the device under individual light illumination, see Fig. S20 (Supporting Information). The

coupled current of the device under simultaneous cooling temperature variation ( $\Delta T = -19.5$  K) and pressure ( $7.6 \text{ kPa}$ ) was enhanced by  $\sim 71.1\%$  when compared with the current of the device under individual cooling, see Fig. S20d (Supporting Information). Under a light intensity of  $83.2 \text{ mW/cm}^2$ , the output current and voltage of the device under simultaneous light illumination and cooling temperature variation ( $\Delta T = -19.5$  K) can be enhanced by about  $375.0\%$  and  $56.3\%$  when compared with the current and voltage of the device under individual light illumination, respectively (Figs. S20e and S20f, Supporting Information).

In order to expand the application of the device, we designed a self-powered multi-functional coupled sensor system by fabricating a  $3 \times 3$  matrix of BTO ceramic wafers. Figs. S21a–S21c (Supporting Information) present the current-time curves of all the channels of the sensor



**Fig. 4.** Output performance of the self-powered multi-functional coupled sensor system. (a–c) Demonstration of mapping the output current of the sensor system under 405 nm illumination through shapes of "Z" (a), "L" (b) and "T" (c). (d,e) Demonstration of mapping the output current of the sensor system during simultaneous application of heating and pressure (d) cooling and pressure (e) through a shape of "T". (f) Demonstration of mapping the output current of the sensor system under simultaneous 405 nm illumination and pressure through a shape of "T". (g,h) Measured output currents of the sensor system under simultaneous application of heating and pressure (g) cooling and pressure through a shape of "T".

system under the application of a cyclic pressure of 33.7 kPa, temperature variations with a heating temperature change of  $\Delta T = 35.1$  K and a cooling temperature change of  $\Delta T = -19.5$  K, respectively. The result indicated that the nine channels of the  $3 \times 3$  sensor system show good output stability, and each channel presented similar current signals as the pressure or temperature variations were turned on and off. By illuminating with 405 nm light to specific channels of the fabricated sensor system through a mask, the current signals could be observed on the mapping figure for the illuminated channels. Fig. 4a–c shows clear “Z”, “L” and “T” shapes in the current output on the mapping image when illuminated with 405 nm light with an intensity of  $83.2 \text{ mW/cm}^2$  on the sensor system through a mask with “Z”, “L” and “T” shape on it. The corresponding output current of the sensor system are displayed in Figs. S22a–S22c (Supporting Information). From the diagram, it can be seen that there is a steady current signal of  $\sim 20$  nA in the illuminated channels, but no current signals in the blocked channels.

Mapping images of the sensor system under the simultaneous application of heating and pressure or cooling and pressure through a shape of “T” are demonstrated in Fig. 4d and e, respectively. It can be clearly seen from the images that the coupled current between cooling and pressure is larger than heating and pressure at the same pressure, which is also illustrated by Fig. 4g and h. Fig. 4f and Fig. S23a (Supporting Information) show the mapping output current and current-time curve of the sensor system under the simultaneous 405 nm illumination and pressure through a shape of “T”. Comparing Fig. 4c with Fig. 4f, it

can be seen that the photovoltaic-piezoelectric coupled effect can be utilized to enhance the output current signals of the sensor system. The output current-time curves and mapping output currents of the sensor system under the simultaneous heating or cooling temperature variations and light illumination through a sharp of “T” as displayed in Figs. S23b, S23c, S23d and S23e (Supporting Information), respectively. The results show that a combination of cooling-light illumination can enhance the current signals of the sensor system, while heating-light illumination can weaken the signal, for the reasons described above.

The fabricated sensor system can be worn on a prosthetic hand to detect light, pressure and temperature variations. Fig. 5a presents an optical image of the sensor system attached to a prosthetic hand, demonstrating high flexibility. Fig. 5b and c shows images of the sensor system attached to a prosthetic hand under illumination by 405 nm light and fingertip pressure. The output current signals of the channels 2 and 3 were measured, as illustrated in Fig. 5d and Fig. S24a (Supporting Information), respectively. The output voltage signals of channel 2 and 3 of the sensor system under different finger pressures are displayed in Fig. S24b (Supporting Information) and the above results indicate that the system can be used to detect the magnitude of light intensity and pressure. Fig. 5e displays an image of ice placed on the sensor system, where the size of the ice exactly covers the area of channel 2. A photograph and infrared image of the sensor system under the combined action of 405 nm illumination and ice cooling is presented in Fig. 5f and g, respectively. The corresponding output current signals of channel 2 of

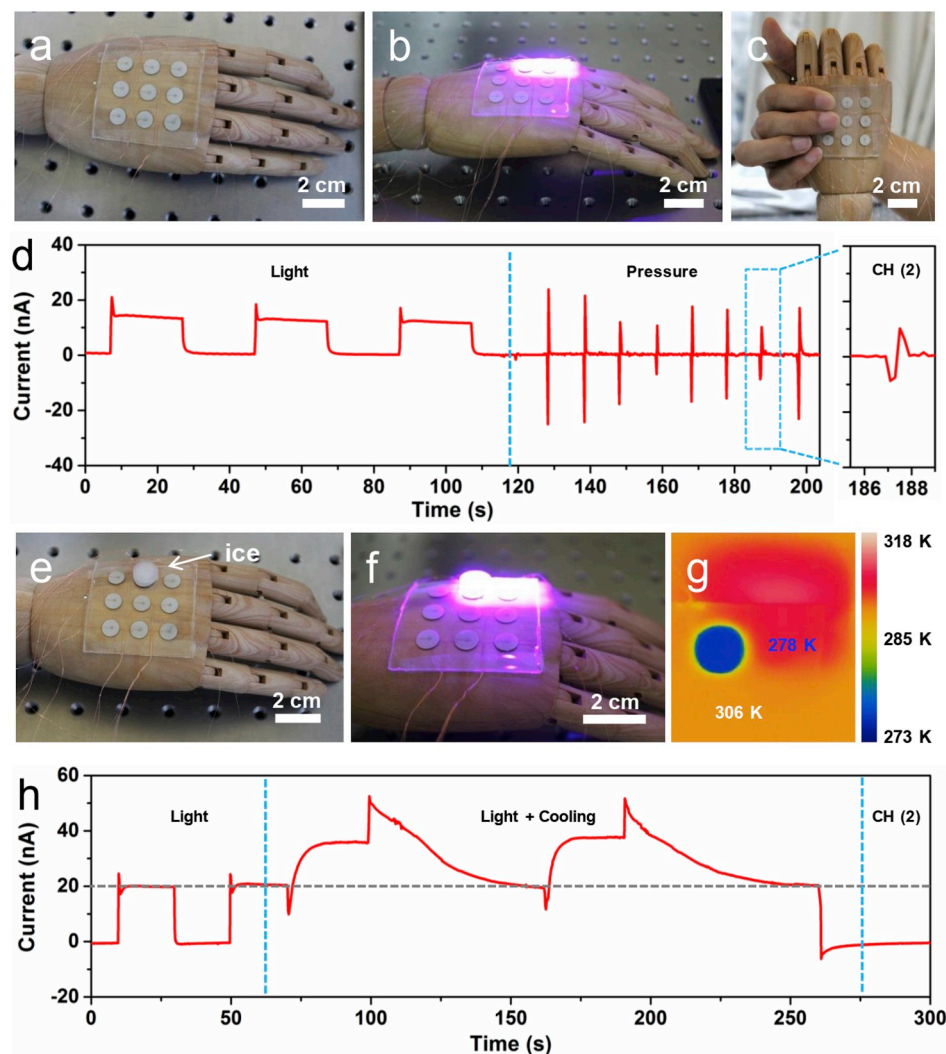


Fig. 5. Application of the self-powered multi-functional coupled sensor system. (a) Optical image of the sensor system attached to a prosthetic hand, demonstrating high flexibility. (b,c) Optical images of the sensor system attached to a prosthetic hand under 405 nm illumination (b) and fingertip pressure (c). (d) Measured output current signals of channel 2 of the fabricated sensor system under 405 nm illumination and finger pressure. (e) Optical image of ice placed on the sensor system. (f) Optical image of the sensor system under simultaneous 405 nm illumination and ice cooling. (g) Infrared image of the sensor system under simultaneous 405 nm illumination and ice cooling. (h) Measured output current signals of channel 2 of the sensor system under conditions of 405 nm illumination only and simultaneous illumination and ice cooling.

the sensor system under the individual 405 nm illumination is approximately 20.2 nA, the simultaneous light illumination and ice cooling increase to 36.8 nA (Fig. 5h). The output current of channel 2 under simultaneous light illumination and ice cooling is calculated to increase by 82.2% compared to individual light illumination. Therefore, the fabricated multifunction coupled sensor system can be successfully implemented for the measurement of light illumination, pressure and temperature changes in the environment.

#### 4. Conclusion

In summary, we have designed a unique one-structure-based multi-effects coupled nanogenerator based on BTO ceramic wafers encapsulated in PDMS. When compared with the individual photovoltaic effect, piezoelectric effect and pyroelectric effect, coupled effects are displayed to have a much larger electrical output. Under a light intensity of approximately 83.2 mW/cm<sup>2</sup>, the coupled current of the device under simultaneous light illumination and pressure (7.6 kPa) can be enhanced by ~ 387.3% when compared with the current of the device under individual light illumination. By applying a cooling temperature change of  $\Delta T = -19.5$  K, the output current signals can be enhanced by over 375.0% under a light intensity of 83.2 mW/cm<sup>2</sup>. Our results reveal the role of coupled effect in BTO nanogenerator and sensor systems, which has potential applications in improving the output performance of coupled nanogenerators based on ferroelectric materials such as hybrid nanogenerators and multi-functional coupled sensors. The nanogenerator was then applied as a self-powered multi-functional coupled sensor system for monitoring variations in light, pressure and temperature. In contrast to conventional multi-function sensor systems, a single pixel of our sensor system is able to simultaneously detect light, pressure and temperature variation which can significantly improve sensor integration level and reduce cost. Moreover, when being mounted on a prosthetic hand, the flexible sensor systems can detect the distribution of light, pressure and temperature variations, exhibiting potential applications as an electronic sensor skin.

#### Declaration of competing interest

The authors declare that they have no known competing financial interests or personal relationships that could have appeared to influence the work reported in this paper.

#### CRediT authorship contribution statement

**Kun Zhao:** Conceptualization, Writing - original draft, Methodology, Investigation. **Bangsen Ouyang:** Conceptualization, Writing - original draft, Methodology, Investigation. **Chris R. Bowen:** Supervision, Validation, Writing - review & editing. **Zhong Lin Wang:** Supervision, Validation, Writing - review & editing. **Ya Yang:** Idea, Supervision, Validation, Writing - review & editing.

#### Acknowledgments

This work was supported by the National Key R&D Program of China (Grant No. 2016YFA0202701), the National Natural Science Foundation of China (Grant No. 51472055), External Cooperation Program of BIC, Chinese Academy of Sciences (Grant No. 121411KYS820150028), the 2015 Annual Beijing Talents Fund (Grant No. 2015000021223ZK32), Qingdao National Laboratory for Marine Science and Technology (No. 2015ASKJ01), and the University of Chinese Academy of Sciences (Grant No. Y8540XX2D2).

#### Appendix A. Supplementary data

Supplementary data to this article can be found online at <https://doi.org/10.1016/j.nanoen.2020.104632>.

#### References

- [1] K. Domanski, E.A. Alharbi, A. Hagfeldt, M. Grätzel, W. Tress, *Nat. Energy* 3 (2018) 61–67.
- [2] G.E. Eperon, T. Leijtens, K.A. Bush, R. Prasanna, T. Green, J.T.-W. Wang, D. P. McMeekin, G. Volonakis, R.L. Milot, R. May, A. Palmstrom, D.J. Slotcavage, R. A. Belisle, J.B. Patel, E.S. Parrott, R.J. Sutton, W. Ma, F. Moghadam, B. Conings, A. Babayigit, H.-G. Boyen, S. Bent, F. Giustino, L.M. Herz, M.B. Johnston, M. D. McGehee, H.J. Snaith, *Science* 354 (2016) 861–865.
- [3] Z. Xiao, Y. Yuan, Y. Shao, Q. Wang, Q. Dong, C. Bi, P. Sharma, A. Gruverman, J. Huang, *Nat. Mater.* 14 (2015) 193–198.
- [4] Z. Li, X. Xu, W. Zhang, X. Meng, Z. Genene, W. Ma, W. Mammo, A. Yartsev, M. R. Andersson, R.A.J. Janssen, E. Wang, *Energy Environ. Sci.* 10 (2017) 2212–2221.
- [5] Y. Yuan, T. Li, Q. Wang, J. Xing, A. Gruverman, J. Huang, *Sci. Adv.* 3 (2017) 1602164.
- [6] Z.L. Wang, J. Song, *Science* 312 (2006) 242–246.
- [7] C. Chang, V.H. Tran, J. Wang, Y.-K. Fuh, L. Lin, *Nano Lett.* 10 (2010) 726–731.
- [8] K. Il Park, J.H. Son, G.-T. Hwang, C.K. Jeong, J. Ryu, M. Koo, I. Choi, S.H. Lee, M. Byun, Z.L. Wang, K.J. Lee, *Adv. Mater.* 26 (2014) 2514–2520.
- [9] R.A. Whiter, V. Narayan, S. Kar-Narayan, *Adv. Energy Mater.* 4 (2014) 1400519.
- [10] J.H. Jung, M. Lee, J.-I. Hong, Y. Ding, C.-Y. Chen, L.-J. Chou, Z.L. Wang, *ACS Nano* 5 (2011) 10041–10046.
- [11] S. Sung-Ho, K. Young-Hwan, L.M. Hyung, J. Joo-Yun, N. Junghyo, *ACS Nano* 8 (2014) 2766–2773.
- [12] Y. Yang, W. Guo, K.C. Pradel, G. Zhu, Y. Zhou, Y. Zhang, Y. Hu, L. Lin, Z.L. Wang, *Nano Lett.* 12 (2012), 2833–2823.
- [13] Q. Leng, L. Chen, H. Guo, J. Liu, G. Liu, C. Hu, Y. Xi, J. Mater. Chem. A 2 (2014) 11940–11947.
- [14] J. Chun, K.Y. Lee, C.-Y. Kang, M.W. Kim, S.-W. Kim, J.M. Baik, *Adv. Funct. Mater.* 24 (2014) 2038–2043.
- [15] J.-H. Lee, H. Ryu, T.-Y. Kim, S.-S. Kwak, H.-J. Yoon, T.-H. Kim, W. Seung, S.-W. Kim, *Adv. Energy Mater.* 5 (2015) 1500704.
- [16] A. Sultana, M.M. Alam, T.R. Mitya, D. Mandal, *Appl. Energy* 221 (2018) 299–307.
- [17] S.B. Lang, *Phys. Today* 58 (2005) 31–36.
- [18] N. Ma, Y. Yang, *Nano Energy* 40 (2017) 352–359.
- [19] W. Satoshi, Y. Koichi, K. Hirofumi, T. Takaaki, K. Takanori, *J. Appl. Phys.* 98 (2005), 014109.
- [20] W.-Q. Liao, Y.-Y. Tang, P.-F. Li, Y.-M. You, R.-G. Xiong, *J. Am. Chem. Soc.* 139 (2017) 18071–18077.
- [21] J. Lim, H. Jung, C. Baek, G.-T. Hwang, J. Ryu, D. Yoon, J. Yoo, K.-I. Park, J.H. Kim, *Nano Energy* 41 (2017) 337–343.
- [22] J. Xing, K.-J. Jin, H. Lu, M. He, G. Liu, J. Qiu, G. Yang, *Appl. Phys. Lett.* 92 (2008), 071113.
- [23] N. Ma, Y. Yang, *Nano Energy* 50 (2018) 417–424.
- [24] H. Fan, C. Chen, Z. Fan, L. Zhang, Z. Tan, P. Li, Z. Huang, J. Yao, G. Tian, Q. Luo, Z. Li, X. Song, D. Chen, M. Zeng, J. Gao, X. Lu, Y. Zhao, X. Gao, J.-M. Liu, *Appl. Phys. Lett.* 111 (2017) 252901.
- [25] Y. Bai, H. Jantunen, J. Juuti, *Adv. Mater.* 30 (2018) 1707271.
- [26] Y. Bai, P. Tofel, J. Palosaari, H. Jantunen, J. Juuti, *Adv. Mater.* 29 (2017) 1700767.
- [27] K. Zhang, Z.L. Wang, Y. Yang, *ACS Nano* 10 (2016) 10331–10338.



**Kun Zhao** received his Ph.D. degree in Material Physics and Chemistry from Beijing Institute of Nanoenergy and Nanosystems, Chinese Academy of Sciences (CAS) in 2018. He is currently an associate professor at State Key Laboratory of Advanced Processing and Recycling of Nonferrous Metals, Lanzhou University of Technology. His main research interests focused on energy harvesting and fabrication of nano-devices, triboelectric nanogenerator, self-powered wireless sensors and new energy technology.



**Bangsen Ouyang** is a Ph.D student in the research group of Professor Ya Yang at Beijing Institute of Nanoenergy and Nanosystems, Chinese Academy of Sciences (CAS). He received his bachelor's degree in Applied Physics from Xihua University in 2014. His current interests focus on self-powered photodetector.



**Prof. Chris R. Bowen** Christopher Rhys Bowen has a BSc degree in Materials Science from the University of Bath (1986–1990) and a DPhil from the University of Oxford (1990–1993). Post-doctoral work was at Technische Universität Harburg-Hamburg and University of Leeds (1994–1996). He was Senior Scientist at the Defence Evaluation and Research Agency from 1996 to 1998. He joined Bath as a Lecturer in 1998 and is now Professor of Materials. Research includes energy harvesting, ferroelectrics and functional ceramics.



**Prof. Zhong Lin (ZL) Wang** received his Ph.D. from Arizona State University in physics. He now is the High tower Chair in Materials Science and Engineering, Regents' Professor, Engineering Distinguished Professor and Director, Center for Nanostructure Characterization, at Georgia Tech. Dr. Wang has made original and innovative contributions to the synthesis, discovery, characterization and understanding of fundamental physical properties of oxide nanobelts and nanowires, as well as applications of nanowires in energy sciences, electronics, optoelectronics and biological science. His discovery and breakthroughs in developing nanogenerators established the principle and technological road map for harvesting mechanical energy from environment and biological systems for powering a personal electronics. His research on self-powered nanosystems has inspired the worldwide effort in academia and industry for studying energy for micro-nano-systems, which is now a distinct disciplinary in energy research and future sensor networks. He coined and pioneered the field of piezotronics and piezophotonics by introducing piezoelectric potential gated charge transport process in fabricating new electronic and optoelectronic devices. Details can be found at: <http://www.nanoscience.gatech.edu>.



**Prof. Ya Yang** received his Ph.D. in Materials Science and Engineering from University of Science and Technology Beijing, China. He is currently a professor at Beijing Institute of Nanoenergy and Nanosystems, Chinese Academy of Sciences, China. He has developed various new hybridized and multi-effects coupled nanogenerators, opening up the new principles of the device design and coupled effects, and the new approaches of improving output performances of energy-related devices. His main research interests focus on the field of hybridized and coupled nanogenerators for energy conversion, self-powered sensing, and some new physical effects.